Periodico di Mineralogia (2014), 83, 1, 55-76 DOI: 10.2451/2014PM0004

PERIODICO di MINERALOGIA
established in 1930

An International Journal of
MINERALOGY, CRYSTALLOGRAPHY, GEOCHEMISTRY, ORE DEPOSITS, PETROLOGY, VOLCANOLOGY
and applied topics on *Environment*, *Archaeometry* and *Cultural Heritage*

Elemental mobility and mass changes during alteration in the Maher-Abad porphyry Cu–Au deposit, SW Birjand, Eastern Iran

Kamal Siahcheshm[1,*], Ali Asghar Calagari[1], Ali Abedini[2] and Sven Sindern[3]

[1]Department of Geology, Faculty of Natural Sciences, University of Tabriz, Tabriz, Iran
[2]Department of Geology, Faculty of Sciences, University of Urmia, Urmia, Iran
[3]Institute of Mineralogy and Economic Geology, RWTH Aachen University, Germany
*Corresponding author: *kl_siahcheshm@tabrizu.ac.ir*

Abstract

The Maher-Abad copper and gold porphyry deposit is located in the east of Iran, and is genetically related to the intrusion of upper Eocene granodiorite into quartz-monzonitic stock and andesitic volcanoclastics. Four types of shell-like and almost concentric alteration zones were developed during three stages, (i) early potassic and propylitic, (ii) transitional phyllic, and (iii) late argillic, where early-formed hydrothermal assemblages have been overprinted by the late ones, temporally. In this study, the mobility of major and some trace elements and changes of mass and volume are considered quantitatively by applying the isocon method of geochemical mass balance within these alteration zones. Isocon plots delineate that the studied alteration system was non-mass-conservative and the mass and volume reduction rate continuously increase from early potassic zone (-2.7% and -5.4%) through phyllic and ultimately to late argillic (up to -7.8% and -15.0%, respectively). Further considerations elucidate that the concentration values of K and Na in the potassic zone reflect the occurrence of hydrothermal biotite and sodic replacement on the rims of plagioclase phenocrysts. Besides, addition of copper and gold to this zone is consistent with Cu-bearing sulfide mineralization. The peculiar geochemical aspect of the propylitic zone is the relative decrease of CaO owing to the high rate of destruction of calcic plagioclase in contrast to the formation of Ca-bearing hydrothermal minerals (e.g., epidote and calcite). In the phyllic zone, both chloritization of biotite and decomposition of plagioclase led to the depletion of ferromagnesian oxides and alkalies (Na_2O and CaO). The addition of Si is consistent with the widespread silicification

which is a major feature of phyllic alteration. All the major oxides were depleted in the argillic alteration zone due to the total destruction of the original ferromagnesian minerals and feldspars.

Key words: mass changes; mobility; alteration; Cu-Au porphyry; Maher-Abad; Iran.

Introduction

Although the porphyry copper deposits have been extensively studied in Mesozoic-Cenozoic orogenic belts of the American Cordillera and the East Pacific Rim (e.g., Sillitoe, 1973; Ahmad and Rose, 1980; Bean and Titley, 1981; Cline and Bodnar, 1991; Dilles and Einaudi, 1992) and their genesis is relatively well understood, few investigations of this style of mineralization have been undertaken in Iran. All known Iranian porphyry copper mineralizations occur in the Cenozoic Central Iranian Tectono-volcanic Belt (Ranjbar et al., 2004) which is also called Sahand-Bazman volcano-plutonic belt (Figure 1). This belt was formed through subduction of the Arabian plate beneath central Iran (upper Cretaceous) during the Alpine orogeny (Paleogene and Neogene) (Niazi and Asoudeh, 1978; Berberian and King, 1981; Pourhosseini,

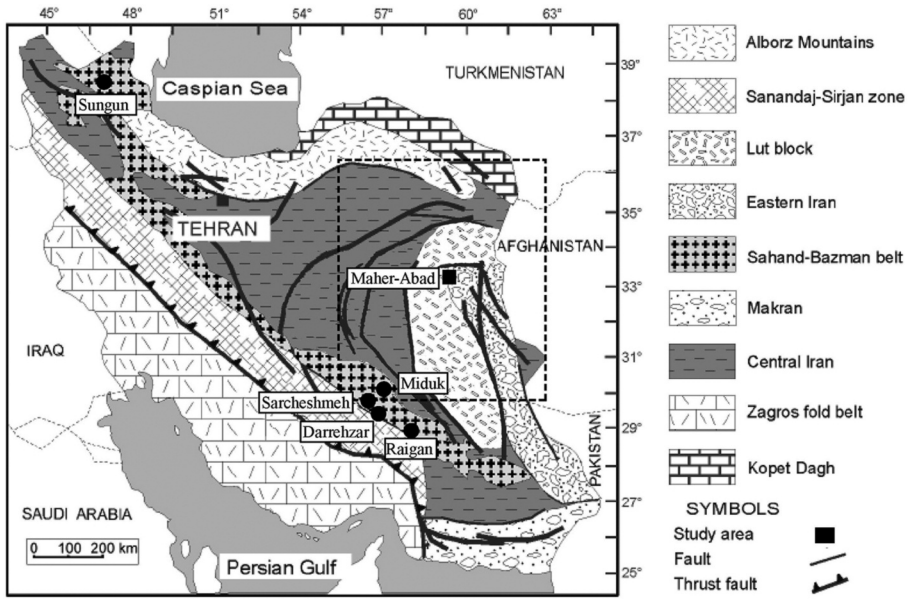

Figure 1. General geological map of Iran showing major lithotectonic units (modified after Nabavi, 1976; Alavi, 1991) and the location of the nation's well-known porphyry copper deposits and the study area in eastern Iran. The window delineates the regional study area (see Figure 2).

1981) and hosts some major porphyry copper deposits including Sungun with 1200 Mt of ore at 0.76% Cu and ~100 ppm Mo (c.f. Calagari, 2004), Sarcheshmeh with 1200 Mt of ore at 0.69% Cu and 0.03% Mo (c.f. Shahabpoor, 2000), Miduk contains 170 Mt of ore at 0.86% Cu, 0.007% Mo, 82 ppb Au and 1.8 ppm Ag (Taghipour et al., 2008; Boomeri et al., 2009), Darrehzar with 49 Mt of ore at 0.64% Cu and 0.004% Mo (c.f. Shafiei and Shahabpour, 2008) and Raigan (Hezarkhani, 2006a) (Figure 1). Recently a few porphyry deposits, outside this belt, were identified by the Geological Survey of Iran. Maher-Abad Cu-Au porphyry deposit is one of these, which is located on the NE the Lut block of Iran. It is a recognized porphyry Cu-Au deposit with respect to its alteration types, mineralization style, geodynamic setting, and igneous rock features. The supergene and hypogene mineralizations possesses inferred average grades of 0.15 % Cu and 0.5 g/t Au (cf. Siahcheshm et al., 2012). Despite the studies done on genetic characteristics of some porphyry copper deposits in Iran, little investigations have been carried out (Calagari, 2003; Hezarkhani, 2006b, 2011) to apprehend the element mobility and mass transfers during alteration vis-a-vis mineralization.

The purpose of this study is to quantitatively assess by applying the Grant's (1986) isocon method of the geochemical mass balance and mass changes of major, minor, and trace elements within the porphyritic stocks (quartz- monzonite and granodiorite) that host the mineralization in the Maher-Abad porphyry copper deposit of the southeastern Iran.

Regional Geology

In the classification of the structural units of Iran (Alavi, 1991; Berberian, 1981; Nabavi, 1976), the Maher-Abad porphyry Cu-Au deposit is situated in the eastern part of the Lut block of the Central Iran (Figure 2) that is in turn a part of the Alpine-Himalayan orogenic belt (Ramazani and Tucker, 2003).

The paleotectonic setting of Lut block is controversial and various scenarios have been defined by different authors. The Lut region reveals a platform character in its sedimentation during the Paleozoic (Tarkian et al., 1983). Intensive orogenic movements during Mesozoic and Tertiary led to breaking and splitting of this platform resulting in a reactivation of different lineaments and finally Central Iran became separated into mosaic blocks after collision with Turan plate (Davoudzadeh and Schmidt, 1984). According to Berberian (1973), the Lut Block is a stable NS-elongate crustal domain extending over 900 km in a NS direction, 200 km wide in EW direction and is a part of the central east Iranian micro-continent.

The calc-alkaline volcano-plutonic rocks of the Lut Magmatic Arc are the result of a west dipping subduction -related closure of Neo-Tethys oceanic plate between the Lut and Afghan blocks in the Tertiary (Karimpour et al., 2005; Richards et al., 2012; Mazhari and Safari, 2013; see Figure 2). Geological observations and Rb-Sr radiogenic isotope data indicate that the oldest magmatic activity in the Central Lut occurred during the Jurassic (165-162 Ma) (Tirrul et al., 1983). The Cenozoic igneous activity in this zone

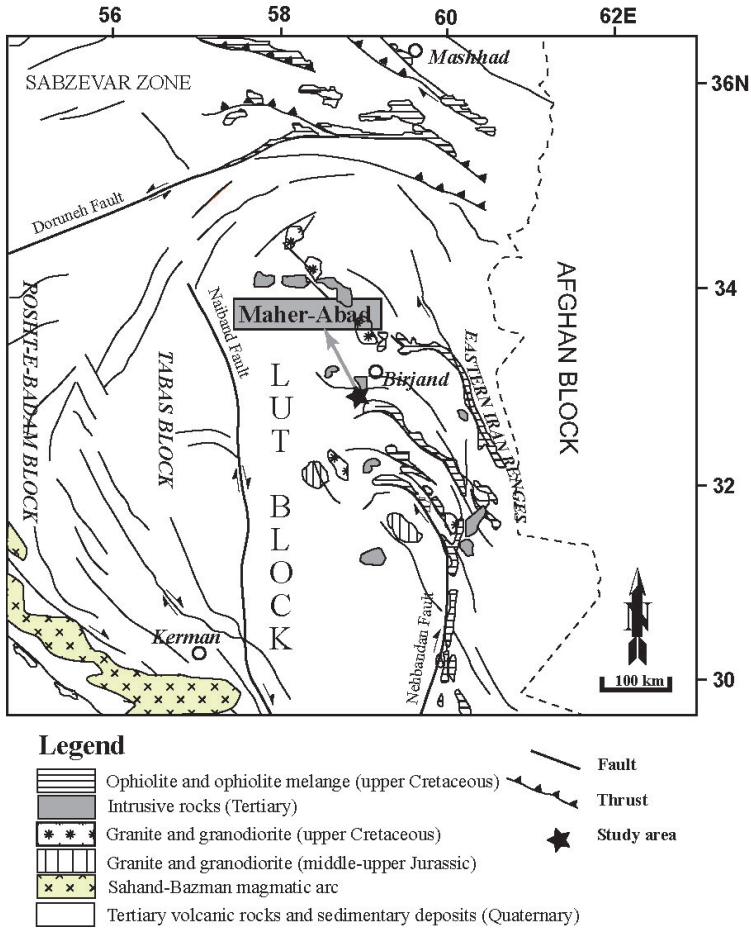

Figure 2. Simplified structural map of Central-East of Iran (Ramazani and Tucker, 2003) and regional geological implications (compiled from Tarkian et al., 1983; Karimpour and Zaw, 2000; Karimpour et al., 2005).

commenced in the middle Eocene (47 Ma) by alkaline and shoshonitic volcanism (Lensch and Schmidt, 1984) continuing and climaxing during the middle-upper Eocene (alkaline and calc-alkaline series; Karimpour et al., 2011). Magmatism continued through Eocene-Oligocene by emplacement of intermediate- acidic porphyritic intrusive rocks (Mahmoudi et al., 2010). The area underlain by the Paleogene volcanics consisting predominantly of andesite and dacite, and their pyroclastic equivalent (tuff and ignimbrite). The intrusive suites are lensoid-shaped characterized by variable age, size, and composition ranging from monzonite to granodiorite. Quaternary sand dunes, salt flats, and alluvial fans cover a large area of the Lut

Block.

The hypabyssal Eocene-Oligocene plutonic rocks are generally associated with extensive copper-gold mineralization events during Tertiary metallogenic episodes in the Lut block producing porphyry copper-gold, iron-oxide copper-gold, vein-type and epithermal gold orebodies as well as many other sub-economic ores (Tarkian et al., 1983; Karimpour and Zaw, 2000; Karimpour et al., 2005).

The mineralized and altered rocks at Maher-Abad district are hosted by three distinct elongate NW-SE trending stocks covering an area of approximately 6 km^2. They are covered by the volcaniclastic rocks. These mineralized and altered stocks range in composition from quartz monzonite to quartz monzodiorite. The most intensely mineralized zone comprises an area of 100×300 m occurring within a conical hill with a surface area of over 1500×1000 m, so called as the Madanha Hill (Figure 3). Further away (~ 300 m) from the Madanha Hill in SW direction, there is another intrusive body called Zardab Hill (with a surface expression 80×180 m). The hornblende-bearing quartz monzonite forms the dominant rock body. The third stock called MH3 Hill is located ~ 400 m in west of Mahanha Hill. It is to be noted, however, that the Zardab and MH3 stocks are shown in regional map of Maher-Abad not in Figure 3.

Methodology

Samples described in this article were mainly collected from outcrops of the alteration zones and also from the diamond-drill core logs of the porphyritic granodiorite and quartz- monzonite wall rocks. Core log samples were initially cleaned ultrasonically (for 20 minutes) by using the method introduced by Chatziliadou et al. (2005). Then 59 samples (altered and least altered) were selected for chemical analyses by XRF (Spectro X-Lab 2000) for major oxides, and by IROES (Infra-red optical emissions spectroscopy) (LECO RC-412) for assessing volatile components (e.g., carbon and sulfur). Furthermore, almost half of these samples (#26) were analyzed by ICP-MS method for minor and trace elements in laboratories at Institute of Mineralogy and Economic Geology, RWTH Aachen University in Germany. After crushing, samples were pulverized and then fused glass disks and pressed powder pellets were prepared for major oxides and trace elements analyses, respectively. Loss-on-ignition (LOI) values were determined on the basis of weighing the analyzed samples before and after two hours of heating at 1150 °C. Organic carbon ($C_{org.}$) and inorganic carbon ($C_{in.}$) were measured at T < 500 °C and T > 500 °C, respectively.

Quantitative chemical analyses of selected minerals (e.g. plagioclase, hornblende, biotite) were carried out by using a JEOL Superprobe JXA-8900R at Institute of Mineralogy and Economic Geology, Germany. Operating conditions were accelerating voltage of 15 kV, probe current of 24 nA, beam diameter of 3-10 μm and a counting time of 20 s for each element analyzed.

XRD analysis of the sample powders were performed with a Bruker D8 Advance Diffractometer by utilizing a Cu-anode. For the

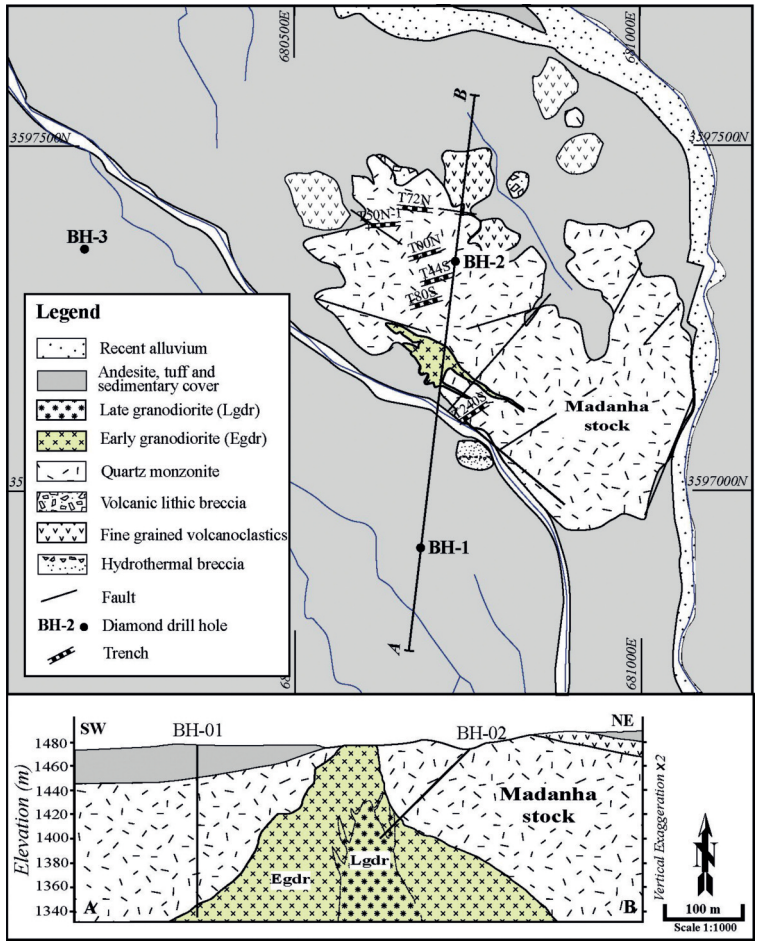

Figure 3. Local geological map of the Maher-Abad porphyry Cu-Au deposit with a cross section along SW-NE trend.

detection of the diffracted X-Rays, the lithium drifted silicon "Sol-X Energy Dispersive X-Ray Detector" was used. The intensity contributions of both Cu $K\alpha_1$ (λ = 1.5406 Å) and Cu $K\alpha_2$ (λ = 1.54439 Å) radiation were recorded, whereas contributions of K-βs are removed from the spectrum. The generator voltage was 40 kV and the current is set to 40 nA.

Geology of the study area

The volcanic-plutonic activities in Maher-Abad area was initiated by the formation of fine-grained andesitic volcaniclastics and volcanic lithic breccias (Figure 3) during the Early to Middle Eocene (Kluyver et al., 1978). The lithic clasts are commonly polymictic,

subrounded to subangular and dominantly of volcanic origin. The andesitic volcaniclastic unit was intruded by a sub-volcanic complex (as closely spaced stocks) ranging in composition from quartz- monzonite to quartz-monzodiorite. The Madanha stock, with an age of 39 ± 0.8 Ma old (U-Pb zircon; Malekzadeh, 2010), appears to be the largest pre-mineralization sub-volcanic intrusion within this area which intruded the coeval andesitic volcaniclastic rocks. They form the major country rocks of the Maher-Abad deposit (Figure 3).

These rock units are intruded by at least two texturally distinct phases of granodiorite porphyries which are referred to as "early granodiorite" and "late granodiorite". However, only the early granodiorite is exposed at Maher-Abad (Figure 3). These phases are differentiated by their contact position, texture, presence of quartz veinlets, the abundance and size of quartz phenocrysts, groundmass characteristics, interception of veinlets, abundance of quartz-sulfide veinlets, and the overall copper-gold grade. However, the diagnostic criteria for discriminating these two phases are their sharp contact and interception of veinlets (quartz-sulfide veinlets within the early phase are cut off by the late granodiorite phase). The granodiorite porphyries form an elongate north-northwesterly trending stock in the central part of the Madanha stock. Maher-Abad Cu-Au porphyry deposit was developed in both porphyritic quartz-monzonite and granodiorite. The copper and gold mineralization appears to be intimately affiliated to the emplacement of these porphyries. The intrusive activity culminates with the emplacement of the late granodiorite (Siahcheshm et al., 2014).

Petrology of the granodiorite porphyries

Based on field and petrographic studies, copper and gold mineralization in the Maher-Abad area is thought to be closely related to the multiple-stage

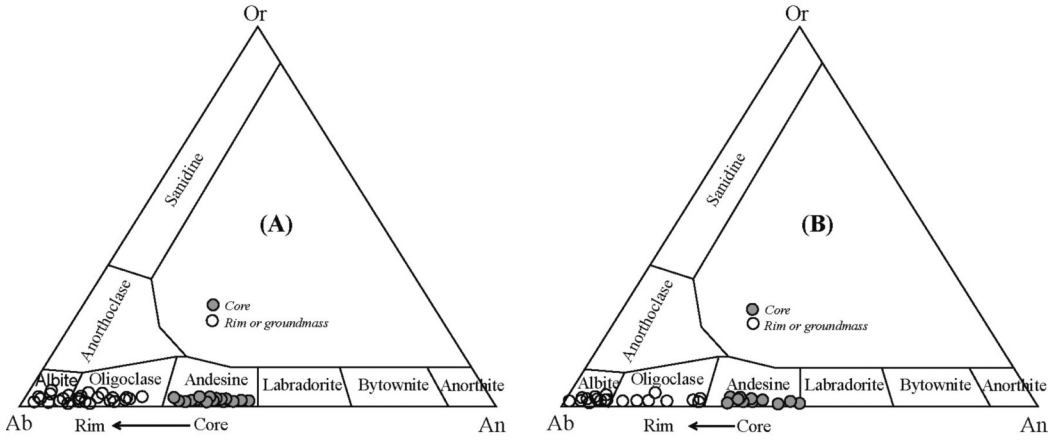

Figure 4. Compositional variation in center and margin of plagioclase phenocrysts. (A) in early granodiorite, (B) in late granodiorite.

Table 1. Summary of hydrothermal alteration and mineralization paragenetic sequences and relative mineral abundances in different vein types of the Maher-Abad porphyry copper-gold deposit.

Least altered (Magmatic)	Early		Transitional	Late (feldspar destructive)
	Propylitic (Chlorite-epidote)	Potassic (Biotite)	Phyllic (Quartz-Sericite-Chlorite)	Argillic (Sericite-paragonite)
Hbl	**Chl**, Cal, *Ep*	**Bt**	**Chl**	Ser+Pg, *Chl*
Bt	**Chl**, Cal, *Ep*	**Bt**	Chl, Bt	
Pl	Pl, **Ep**, Cal	**Pl,** *Cal, Anh*	**Ser,** Pl, **Cal**	**Ser,** Pg, **Kln, Ilt, Mnt**±Dkt±Sme
K-feldspar	Or, Ser	Or, Ser	**Ser**	Ser, clay minerals
Sulphides	*Py disseminated/veinlets*	**Py, Ccp, Bn**± Dg	**Py,** Ccp, *Bn*± *Po*	Py, Gn
Veins and Veinlets	*B veinlets* (**Qtz**+Py)±Chl	**A** (**Qtz**+Py+Ccp), Ab (Qtz+Bt ±Kf), Ac (**Qtz+Py+Cal**), **C** (**Py+Ccp+Bn**+Dg) veinlets	Ac, **B,** *D* veins/veinlets	**D** veinlets (Cal+Qtz+Py), Clay minerals ±Ser±Gn
Primary rock texture				
	← *increasing in distance*	*center of Porphyry system*	*increasing in distance* →	
	Preserved		Destroyed	

Notes: Quartz is ubiquitous; bold font indicates high abundance; regular font indicates moderate abundance; italics font indicates minor or rare abundance.

Mineral abbreviations: Anh - Anhydrite, Bt - biotite, Bn - bornite, Cal - calcite, Ccp - chalcopyrite, Chl - chlorite, Dg - digenite, Dkt - dickite, Ep - epidote, Gn - galena, Hbl - hornblende, Hem - hematite, Ilt - illite, Kln - kaolinite, Mnt - montmorillonite, Or - Orthoclase, Pg - paragonite, Pl - plagioclase, Py - pyrite, Ser - sericite, Sme - smectite.

intrusion of granodiorite porphyries. The mineralogy of the early and the late granodiorite porphyries is almost identical, and includes phenocrysts (40-50 vol.% of the rock) of plagioclase, hornblende, biotite and quartz. The phenocrysts are set in a fine- to medium-grained groundmass of mainly quartz, K-feldspar, albite, and opaque minerals (Table 1).

According to the electron probe micro-analyses, the plagioclase phenocrysts in the early granodiorite have An_{50-30} at the core and An_{30-2} near the rim (Figure 4A). In fact, the plagioclase composition varies systematically from core (andesine) through inner rim (oligoclase) to outer rim (albite). The compositional trend (from core to the rim) of plagioclase phenocrysts in the late granodiorite is similar (An_{50-2}) to those of the early granodiorite (Figure 4B).

The hornblende phenocrysts have a low mole fraction of Fe^{+2} (XFe^{+2} = 0.14-0.18; Figure 5a). This is similar to those reported (e.g., Imai, 2000, 2001) from intrusive rocks associated with porphyry Cu mineralization elsewhere in the world.

The late granodiorite is less altered than the early granodiorite and is readily identifiable by the presence of phenocrysts of medium-sized "quartz eye" (< 2 mm) and coarser (> 2 mm) biotite and hornblende. The magmatic biotite phenocrysts are texturally euhedral to subhedral with reddish-brown to green color and range in size from 1 to 4 mm. These biotites are observed in both least-altered and altered samples (potassic and phyllic alteration zones) (Figure 6 a,b,c,f). The secondary hydrothermal biotite occurs as flaky aggregates in granodiorite and is petrographically distinct from the primary (magmatic) one. The primary biotites in the granodiorite porphyries have phlogopitic

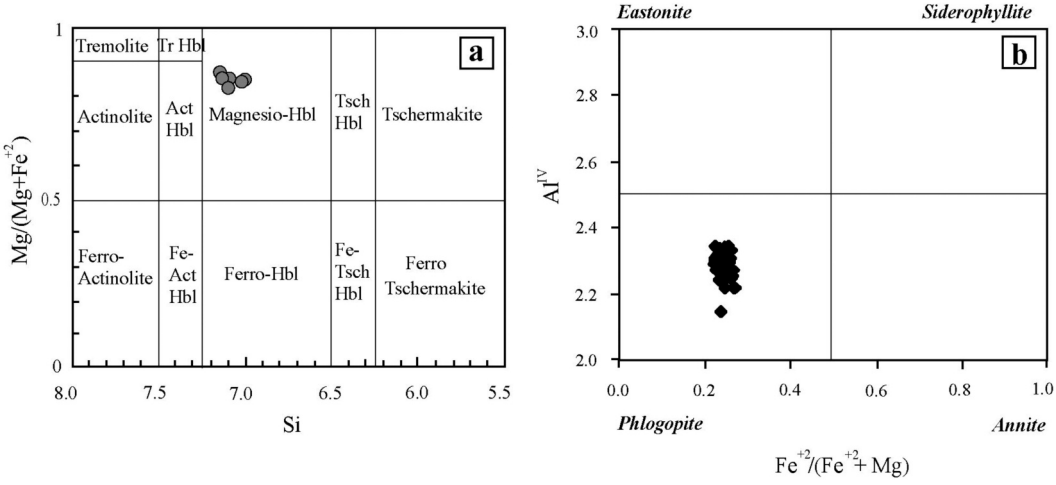

Figure 5. Chemical composition of biotites and hornblendes of granodiorite porphyry. (a) Mg-rich hornblende, based on Hawthorne (1981). (b) Phlogopitic biotite, based on Rieder et al. (1998).

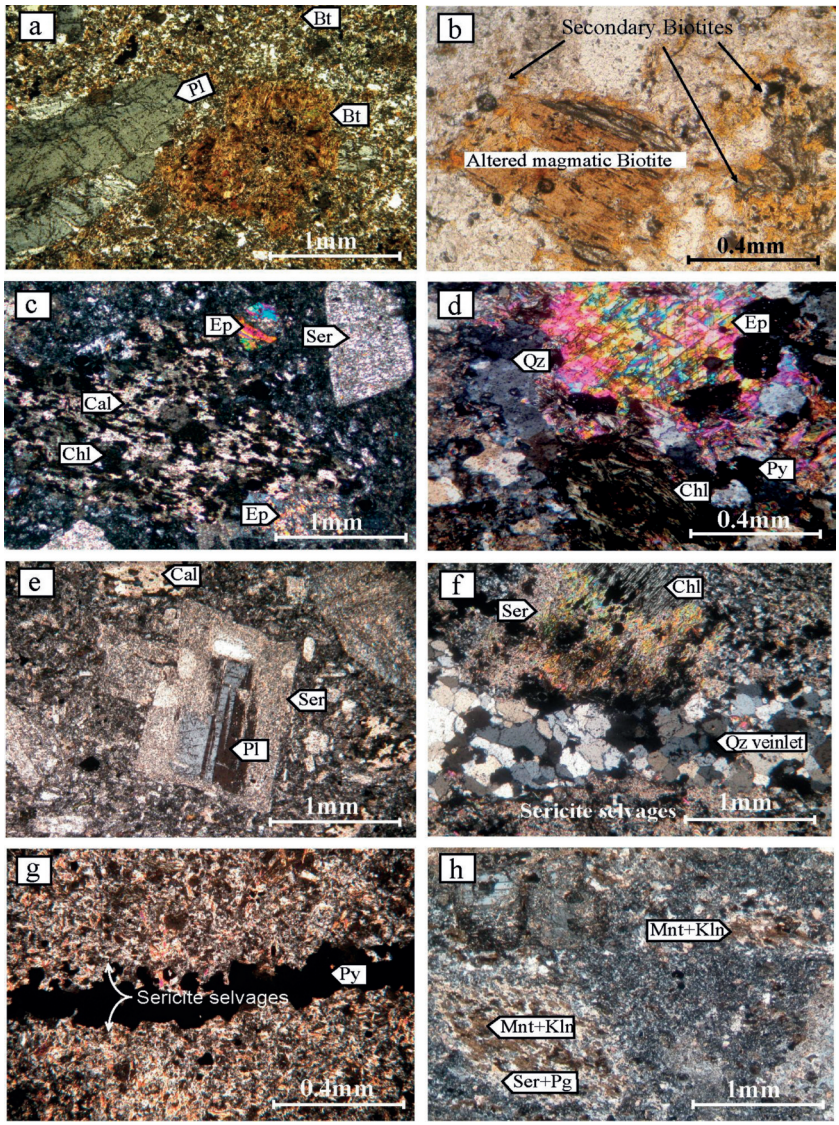

Figure 6. Photomicrographs of various alteration zones. (a) Alteration of ferromagnesian minerals to secondary biotite and Fe-oxides (XPL) in potassic zone. (b) Gradual alteration of magmatic biotite to fine 'flaky' secondary biotite (PPL) in potassic zone. (c) Alteration of plagioclase to epidote and replacement of hornblende phenocryst by chlorite and calcite (XPL) in propylitic zone. (d) Formation of epidote within plagioclase crystals and replacement of ferromagnesian minerals by chlorite (XPL) in propylitic zone. (e) Alteration of plagioclase crystals to sericite (XPL) in phyllic zone. (f) Selective replacement of mafic minerals by sericite and chlorite (XPL) in phyllic zone. (g) Pyrite veinlets with sericitized boundaries (XPL) in phyllic zone. (h) Alteration of ferromagnesian minerals to sericite-paragonite and kaolinite (XPL) in argillic zone. Abbreviations for minerals are from Whitney and Evans (2010).

composition with X_{Mg} ranging from 0.73 to 0.78 (Figure 5b) corresponding to a mole fraction range X_{Phl} = 0.67-0.72 (Siahcheshm et al., 2012).

Alteration

The hydrothermal alteration at Maher-Abad is characterized by four main concentric shell-shaped zones developed in three temporally and spatially overlapping stages: (1) the early, (2) the transitional, and (3) the late. The pattern of alteration zones is almost similar to those of typical ones developed around other porphyry Cu deposits (Lowell and Guilbert, 1970; Titley and Beane, 1981). The early hydrothermal alteration consists of a central potassic inner core and peripheral propylitic zones occurring in both the granodiorite (hosting mineralization) and wall rocks (quartz-monzonite and andesitic volcanoclastics). The transitional and the late stages referred to as "feldspar destructive alteration" have typically encroached downward and overprinted the early stage alteration assemblages (Table 1).

Potassic alteration

This zone occurs in deeper parts of Maher-Abad porphyries (by referring to the location of core log samples taken from this zone) and hence it is not cropped out at surface. The samples from this zone in granodiorite have typically brownish grey color in hand specimen, and include plagioclase (An_{60-10} from core to rim), biotite (primary and secondary) (10-20%), quartz, pyrite, chalcopyrite, and scattered magnetite. The medium- to coarse-grained plagioclases are locally replaced by very fine grained sericite. The hydrothermal alteration products generally occur widely as groundmass replacement, veinlets, and interstitially within plagioclase, hornblende, and primary biotite phenocrysts. The hydrothermal biotite commonly occurs as fine-grained (10-100μm) flaky aggregates principally replacing earlier mafic minerals (Figure 6a) and/or is present as disseminated flakes in the matrix (Figure 6 a,b) and veinlets. They have phlogopitic composition with X_{Mg} ranging from 0.70 to 0.78 corresponding to X_{Phl} = 0.63-0.73 (Siahcheshm et al., 2012). The mineralization is manifested by the presence of primary copper-bearing sulfides which mostly occur as disseminated grains or associated with the early to transitional "A", "Ac", "C" veinlets (see Table 1). The earliest "A" and "Ab" veinlets typically display discontinuous pattern, irregular wall-rock contacts and granular texture. The characteristics of the veinlets suggest a plastic rather than brittle fracturing (cf. Gustafson and Hunt, 1975; Muntean and Einaudi, 2001). The plastic nature of the veinlets in potassic zone may indicate their formation under lithostatic regime (cf. Founier, 1999).

Propylitic alteration

The mineral assemblages within propylitic zone are typically characterized by the presence of chlorite replacing hornblende and biotite, and of epidote replacing plagioclase (Figure 6d). The propylitic-related quartz + pyrite (± chlorite) veinlets typically show continuous pattern with regular wall-rock contacts.

Phyllic alteration

Almost all rock types within Maher-Abad

deposit, especially quartz- monzonite stock as well as early granodiorite have been pervasively affected by phyllic alteration. It is widely observed at surface outcrops as well as in most diamond drill core samples. Sericite, chlorite and minor calcite along with quartz veins/veinlets constitute the phyllic alteration assemblage. Associated with this zone are also pyrite (± chalcopyrite) vein/veinlets in deeper parts of this zone. Quartz-sulfide "B" veins/veinlets (0.1-6 cm width) are associated with this zone (Table 1), and commonly exhibit continuous pattern with regular wall-rock contacts. Though partially chloritized, there are some relic magmatic and/or hydrothermal biotites in a few samples (Figure 6f).

Argillic alteration

In this zone, silicate minerals are affected by both supergene and hypogene alteration events. The late argillic alteration is characterized by nearly complete destruction and replacement of pre-existing mafic minerals (e.g., hornblende, biotite) and feldspars by fine to medium-grained white micas,(i.e., muscovite, paragonite), clay minerals (kaolinite, illite-sericite, montmorillonite), quartz, and iron hydroxide. Because pyrite and alumino-silicates dominate in phyllic zone, descending oxidizing fluids may become more acidic and develop clay minerals and iron hydroxides with supergene origin (cf. Titley and Marozas, 1995).

Mineralization

The hypogene copper and gold mineralization in Maher-Abad deposit is zoned around the granodiorite porphyries and centered mostly in the potassic core and slightly in the phyllic alteration zones. The ore mineralization is characterized by the presence of the hypogene copper-bearing sulfides. The copper sulfides occur as finely disseminated grains in the groundmass and as fracture coatings associated with the early mineral assemblages and quartz veinlets. The Cu-sulfides are mainly chalcopyrite, digenite, and bornite (Table 1). Pyrite is the most abundant sulfide and chalcopyrite is the main copper ore mineral. Chalcopyrite occurs as disseminated grains within the matrix and quartz-sulfide veinlets where it preferentially replaces pyrite and is typically replaced by bornite. Gold occurs as very fine inclusions within the sulfide grains as well as 'free' gold along quartz and/or silicate grain boundaries. The supergene sulfides are characterized by digenite and covellite replacing partially to entirely chalcopyrite and bornite.

Discussion

Many methods are used for calculation of mass loss or gain in mineral deposits including methods such as (1) volume factor (Gresens, 1967), (2) immobile elements (MacLean and Kranidiotis, 1987; MacLean, 1990; Nesbitt and Markovics, 1997), and isocon (Grant, 1986). Gresen's method (1967) which was revised by Grant (1986) made possible the variations of elements and oxides to be illustrated in the isocon diagram. Therefore, this method was used for calculation of mass exchange variations in Maher-Abad deposit. Mass and volume changes were calculated on the basis of concentration values of immobile elements in altered samples versus those of corresponding

elements in least altered ones (as precursor). Thus, selection of immobile elements is very crucial and their lack of relative mobility should be carefully assessed in analyzing the effects of mass exchange. The average chemical compositions of quartz-monzonitic and granodioritic porphyries of least altered and some other altered samples belonging to various alteration zones are listed in Table 2.

Immobile elements

Studies revealed that trace elements like Ti, Al, and Zr behave relatively immobile during hydrothermal alteration and are often used as a basis for calculation of mass exchange in many copper and gold porphyry deposits (Ulrich and Heinrich, 2002). For determination of immobile elements, it is customary that the selective elements are plotted against TiO_2 and those having correlation coefficient ≥ 0.6 are chosen (MacLean and Kranidiotis, 1987; Bühl and Zöfel, 1999). Calculations of correlation coefficients among elements show that there are positive correlations among elements such as Al, Dy, Yb, Lu, Nb, Zr, Hf, Ti, and Ga (r = 0.6-0.8) in altered and least altered rocks. Thus, Al, Ti, Zr, Ga, Hf, Nb, and HREEs (e.g. Dy, Yb, Lu) are considered to be as immobile elements in alteration zones at Maher-Abad and employed as index elements for mass exchange in this study.

Calculation of mass equilibrium

For implementing these calculations, isocon plots with logarithmic axes (proposed by Baumgartner and Olsen, 1995) are illustrated. Immobile elements are used for determination of an isocon line, and for this purpose the standard deviations should be taken into account (Selverstone et al., 1991; Leitch and Lentz, 1994). The slope of isocon lines are defined as the ratio of the mass of fresh (or least altered) parent rocks to that of the altered rocks (M^o/M^a). When the position of immobile elements is determined, the geochemical variations of the elements from the viewpoint of their relative mobility (either increase or decrease) are discussed. That is, elements plotted above the reference isocon line are enriched and those that lie below the line are depleted during alteration processes. Absolute compositional variation (ΔC) is defined as the ratio of concentration value of each element in altered rock (C_i^a) to that of corresponding element in its precursor (C_i^o). These calculations are carried out by the following equation (Grant, 1986; 2005):

$$\Delta C_i/C_i^o = (M^a/M^o)\times(C_i^a/C_i^o) - 1 \quad \text{(Equation 1)}$$

This equation can be written as follows (Idrus et al., 2009):

$$\Delta C = (1/S)\times(C^a/C^o) - 1 \quad \text{(Equation 2)}$$

In above equation, S is the isocon gradient of immobile element and C^a/C^o) is the ratio of concentration value of an element in altered sample to the corresponding element in its precursor (least altered). Quantitative values of volume and mass changes are calculated according to the following equations (Grant, 1986; Idrus et al., 2009):

$$\Delta V\ (\%) = [(1/S)\times(\rho^a/\rho^o)-1]\times 100 \quad \text{(Equation 3)}$$

$$\Delta M\ (\%) = [(1/S)-1]\times 100 \quad \text{(Equation 4)}$$

ΔV and ΔM are values of increment or

Table 2. Whole-rock geochemical data (mean) of various fresh/least and hydrothermally altered rocks associated with different rock units.

major oxides/ elements	Fresh/least altered rocks			Potassic zone			Propylitic zone zone		Pyllic	Argillic zone
	Egdr (N=2)	Lgdr (N=2)	Qmz (N=3)	Egdr (N=10)	Lgdr (N=9)	Qmz (N=8)	Qmz (N=6)	Vfg (N=4)	Qmz (N=8)	Qmz (N=7)
SiO_2	68.88	70.33	61.81	69.61	69.33	63.84	57.26	56.83	68.89	64.01
TiO_2	0.28	0.31	0.69	0.31	0.26	0.46	0.71	0.72	0.45	0.59
Al_2O_3	14.02	13.50	15.25	14.13	14.79	16.50	17.96	17.69	15.88	17.76
FeO	4.95	3.65	5.83	4.30	3.78	6.19	8.30	8.72	3.55	5.93
MnO	0.05	0.06	0.14	nd	0.11	nd	0.22	0.23	nd	nd
MgO	0.86	0.89	3.48	0.91	0.84	1.93	3.72	3.14	2.02	1.69
CaO	3.12	4.33	5.32	1.54	2.16	2.73	5.25	5.77	1.40	0.71
Na_2O	4.46	4.06	3.66	4.77	3.99	4.31	2.04	2.41	2.38	2.54
K_2O	2.21	2.62	3.46	4.51	2.16	2.89	1.83	1.59	2.98	2.33
P_2O_5	0.14	0.17	0.20	0.12	0.13	0.16	0.15	0.14	0.22	0.17
LOI	1.16	1.07	1.54	1.05	2.02	1.81	4.02	4.22	2.67	5.74
Total	100.13	100.97	101.39	101.25	99.57	100.80	101.46	101.44	100.43	101.48
Density	2.67	2.65	2.73	2.60	2.62	2.61	2.67	2.69	2.55	2.35
S	0.07	0.02	0.32	0.19	0.20	0.35	0.16	0.09	0.51	1.48
C	0.16	0.19	0.11	0.30	0.27	0.18	0.41	0.21	0.23	0.12
Cr	29.50	161.00	94.23	5.75	15.67	26.00	18.83	9.00	18.00	16.85
Co	7.60	5.70	13.33	18.09	9.92	15.52	17.13	20.85	10.22	22.03
V	52.00	40.00	139.33	58.81	41.10	71.54	157.17	134.98	70.17	98.78
Cu	1170.48	136.96	164.97	4694.61	1411.25	1790.94	148.06	173.52	928.64	660.98
Pb	37.00	12.50	24.00	48.80	37.00	36.50	39.20	36.00	35.38	51.43
Zn	89.30	104.90	79.92	57.31	57.32	57.51	86.00	99.89	65.50	85.81
Sn	2.00	2.00	1.67	1.89	2.15	1.84	2.50	3.50	1.50	3.59
Mo	3.00	2.00	2.50	nd	nd	nd	bd	bd	1197.00	66.40
As	1.38	1.63	3.65	nd	1.65	1.45	bd	7.75	1.50	1.98
Se	2.65	1.00	0.50	7.54	0.65	1.03	bd	1.67	1.80	3.90
Au	365.25	40.00	25.33	1212.25	221.50	84.75	9.50	nd	21.25	15.00
Rb	24.00	14.00	33.33	29.87	36.36	18.61	16.33	14.63	16.00	27.62
Ba	412.00	554.50	668.67	277.15	381.34	239.84	241.33	106.70	316.04	226.46
Sr	370.50	477.50	534.33	272.28	296.13	354.87	285.00	305.72	338.25	94.03
Ga	15.00	18.00	16.00	18.91	18.04	19.44	19.40	17.10	19.67	19.24
Hf	1.35	1.90	1.73	1.25	2.33	2.67	2.00	2.50	1.95	2.22
Zr	54.50	57.00	65.00	47.91	45.89	59.70	43.50	65.84	52.20	63.91
Nb	1.10	1.45	1.97	3.45	2.00	2.00	2.00	1.50	2.00	1.75
Y	6.00	8.50	12.33	3.00	7.50	6.50	12.50	15.00	8.00	10.82
Th	0.52	1.40	0.79	0.40	2.25	0.75	1.10	0.75	0.80	0.68
U	0.08	0.33	0.39	0.10	0.45	0.20	0.35	0.30	0.30	0.23

Notes: Major oxides, LOI (Loss on Ignition), S and C are in wt%, all trace elements are in ppm with the exception of Au in ppb, and density is in g/cm^3; abbreviation of rock types: Egdr-early granodiorite, Lgdr= late granodiorite, Qmz = quartz-monzonite and Vf g = andesitic volcaniclastic rocks. N = numbers of analyzed samples; nd = not detected.

Table 2. Continued ...

major oxides/ elements	Fresh/least altered rocks			Potassic zone			Propylitic zone zone		Pyllic	Argillic zone
	Egdr (N=2)	Lgdr (N=2)	Qmz (N=3)	Egdr (N=10)	Lgdr (N=9)	Qmz (N=8)	Qmz (N=6)	Vfg (N=4)	Qmz (N=8)	Qmz (N=7)
La	10.05	12.25	20.79	11.30	13.05	12.10	17.98	8.63	15.52	12.97
Ce	19.73	24.44	39.42	12.87	17.59	24.62	34.47	11.40	32.97	17.60
Pr	1.97	1.97	3.68	1.29	4.74	2.31	3.11	1.53	3.29	2.39
Nd	8.47	8.15	17.16	2.00	8.42	11.59	12.79	2.20	11.41	7.16
Sm	1.38	1.72	2.53	1.00	1.45	1.40	2.17	9.47	2.20	1.59
Eu	0.55	0.57	0.87	0.44	0.47	0.51	0.82	0.83	0.68	0.47
Gd	1.51	1.61	2.40	1.15	1.20	1.20	2.13	2.30	2.05	1.13
Tb	0.24	0.24	0.40	0.16	0.18	0.20	0.33	0.40	0.30	0.17
Dy	1.41	1.35	2.30	1.11	1.05	1.10	1.84	2.45	1.95	0.80
Ho	0.24	0.28	0.46	0.58	0.20	0.20	0.39	0.50	0.40	0.16
Er	0.74	0.90	1.50	0.58	0.77	0.75	1.16	1.60	1.45	0.41
Tm	0.12	0.16	0.22	0.09	0.13	0.11	0.16	0.25	0.20	0.08
Yb	0.75	1.05	1.40	0.56	0.85	0.75	1.08	1.55	0.85	0.55
Lu	0.12	0.17	0.19	0.09	0.14	0.12	0.18	0.23	0.19	0.09

Notes: Major oxides, LOI (Loss on Ignition), S and C are in wt%, all trace elements are in ppm with the exception of Au in ppb, and density is in g/cm^3; abbreviation of rock types: Egdr-early granodiorite, Lgdr= late granodiorite, Qmz = quartz-monzonite and Vf g = andesitic volcaniclastic rocks. N = numbers of analyzed samples; nd = not detected.

decrement in volume and mass, respectively. ρ^a/ρ^o is the ratio of density (g/cm^3) of altered sample to that of its precursor (least altered).

Mass changes during alteration

Alteration reactions are accompanied with depletion of some elements from the rock and simultaneous addition of some others. The relations between the precursor (least altered) and its alteration products are determined on the basis of mass increase or decrease of major elements. Depletion of an element normally occurs as the result of decomposition of minerals in the precursor rocks and its simultaneous leaching by the fluid phase during progressive alteration (Aiuppa et al*.,* 2000; Kirschbaum et al., 2005). This element may redistribute in the other parts of the alteration system and is deposited, consequently its concentration value may increase. The conservation rate of each element in alteration zones is dependent on the degree of stability of initial minerals of the host rocks and also on the possibility of formation and stability of secondary minerals being capable of hosting this element.

Potassic (biotite) zone

The average chemical composition of granodiorite samples that suffered potassic alteration relative to that of the corresponding least altered samples indicates that immobile elements have an isocon line with a slope of 1.03 exhibiting trivial mass and volume decrease -2.75% and -5.43%, respectively (Figure 7a). Samples from this zone display a remarkable rise in K_2O, S, and

C and to some extent in MgO and Na_2O, whereas Fe_2O_3 and CaO illustrate decreasing trends (Figure. 7b). The minor Fe_2O_3 loss is due to the partial leach of Fe from this zone. Rb shows a consistent increase with K_2O and is related to the abundance of secondary biotite in this zone. Minor Na_2O gain may be related to Na substitution for Ca in plagioclase rim. Sr decrement can be attributed to the decomposition of plagioclase. Plagioclase is also replaced by sericite and there are secondary biotite which can hold Ba. It appears that replacement of Ca-rich hornblende (CaO = ~10 wt%) by the secondary biotite led to the decrease of CaO in these rocks, and it is presumed that the released CaO from hornblende during biotitization furnished the essential ingredient for the formation of calcite and epidote in distal parts of the deposit. As expected, copper and gold (with enrichment factors of 2.90 and 2.23, respectively) show significant increase. This conforms with the abundance of Cu-bearing sulfides such as chalcopyrite, bornite, and digenite.

Propylitic (chlorite-epidote) zone

Quartz- monzonite that suffered propylitic alteration is observed mainly in the peripheral part of the deposit and the corresponding samples exhibit mass and volume reduction -2.26% and -4.47%, respectively (Figure 7c) relative to that of the least altered rocks. This may be related to the leaching of major oxides such as SiO_2, Na_2O, K_2O, and sulfur from the rocks. The peculiar geochemical characteristics of this alteration zone are the substantial enrichment of CO_2 (approximately two times) and relative decrease of CaO (Figure 8d). Therefore, it can be conceived that the leaching of Ca from the calcic plagioclase is more effective than its fixation as Ca-bearing silicates (*e.g.,* epidote) and carbonate (*e.g.,* calcite). Reduction of Rb, Ba, and Sr can be attributed to the depletion of K_2O and Na_2O. Loss of Na_2O and K_2O is likely due to the decomposition of plagioclase and lack of secondary biotite in this zone.

Phyllic (quartz-sericite-chlorite) zone

Samples of this zone were normalized to that of potassic alteration zone, because the potassic zone is conceived to be superimposed by transitional phyllic zone and hence can be regarded as a precursor for this zone. Samples of this zone show mass and volume decrease -2.37% and -4.69%, respectively (Figure 7e). SiO_2 increase can be ascribed to the presence of thick quartz-sulfide veinlets being a characteristic feature of this zone. Chloritization of the primary biotite 'books' and decomposition of plagioclases led to the decrease of total Fe, Na_2O, and CaO. Sericitization of feldspars and ferromagnesian minerals, however, caused a minor increase in K_2O value. CO_2, S, Zn, Pb, and Ba are relatively added. Copper and gold grade show a decreasing trend relative to the potassic zone, as abundance of Cu-bearing sulfides decreases (Figure 7f). The addition of Si is consistent with widespread silicification (forming quartz veins/veinlets) which is a major feature of phyllic alteration.

Argillic (kaolinite - paragonite - quartz) zone

The transitional phyllic zone was conceived to

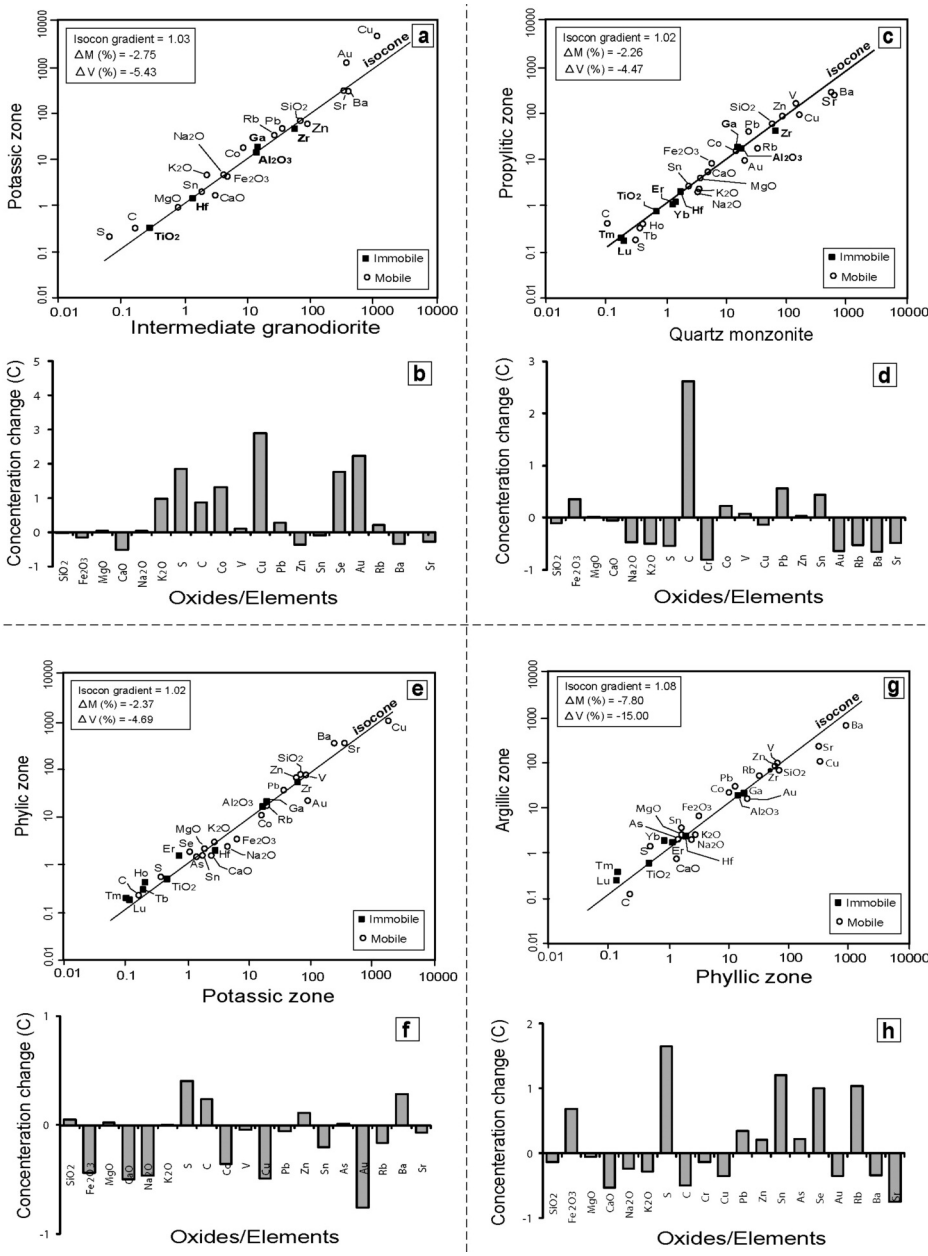

Figure 7. Plots of mass exchanges among various alteration zones by using isocon method along with diagrams of compositional variations of elements (ΔC) in various alteration zones. (a,b) In the potassic zone (N=10) relative to least altered early granodiorite (N=2). (c,d) In the propylitic zone (N=10) compared to the least altered quartz-monzonitic rocks (N=2). (e,f) In the phyllic zone (N=8) compared to the potassic zone (N=8) in quartz-monzonite. (g,h) in the argillic zone (N=7) relative to the phyllic (N=8).

precursor for the argillic zone. Samples from this zone show considerable mass and volume loss -7.8% and -15.00%, respectively (Figure 7g) owing to the total destruction of initial mafic minerals and plagioclase. It is quite evident that if the samples of this zone were normalized to the least altered rocks, the mass and volume losses would be much greater than these values. Except Fe_2O_3, which is a little added (Figure 7h), almost all major oxides were depleted. CO_2 is generally depleted in this zone whereas sulfur shows an enrichment factor of 1.67. The mass gain of Fe_2O_3 and sulfur are consistent with the abundance of pyrite. Although the values of CaO, Na_2O, and K_2O encounter a total decrease in analyzed samples, CaO displays relatively more depletion than the other two. This may be owing to the fact that the plagioclase destruction occurred in a higher rate relative to the leaching of K_2O and Na_2O which have the potential of fixation in sericite and paragonite. Rb is relatively enriched likely due to its fixation in sericite and paragonite whereas Ba and Sr were leached mainly because of destruction of feldspars. Pb, Zn, As, Sn, and Se are increased, but copper and chromium are diminished.

Conclusion

The important results obtained from the consideration of the behavior of immobile elements during alteration and mineralization in Maher-Abad porphyry Cu-Au deposit are as follows:

1 Isocon plots illustrate that trace elements such as Al, Ti, Zr, Ga, and HREEs were relatively immobile during alteration processes.

2 In the course of transition from initial alteration zone (potassic and propylitic) through phyllic and ultimately to late argillic, the mass and volume reduction rate continuously increased. These variations may be affiliated with total decrease of elemental activities in hydrothermal fluids during alteration.

3 Rocks with potassic alteration display K and Na enrichment due to formation of hydrothermal biotite and marginally sodic replacement of Ca in plagioclase. Values of Si, CO_2, S, Cu, and Au show also mass gains whereas Ca and to some extent Sr and Ba are leached as the result of decomposition of hornblende and plagioclase. Copper mineralization occurred as dissemination and veinlets (quartz-sulfide) and is characterized by the copper-bearing sulfides such as chalcopyrite, bornite, and digenite. The gold enrichment may be justifiable by assuming its presence as inclusions within sulfide grains and/or along grain boundaries of quartz and other silicates.

4 Propylitic zone is accompanied with relative reduction of Na_2O, K_2O, CaO, Rb, Ba, and Sr that may be as the result of high degree of decomposition of calcic plagioclase and lack of secondary biotite in this alteration zone.

5 Due to the presence of thick quartz-sulfide veinlets in the phyllic alteration zone, values of SiO_2 (owing to sericitization of feldspars and ferromagnesian minerals) and K_2O (due to fixation in sericite) show mass increase. Chloritization of primary biotites and decomposition of plagioclase, however, caused the reduction of ferromagnesian oxides and

alkalies (e.g., Na_2O and CaO).

6 The altered samples from the argillic zone are almost depleted in major oxides (ferromagnesian and alkali elements). This could be related to total destruction of primary mafic minerals and plagioclase, and hence with considerable mass and volume reduction -7.80% and -15.00%, respectively. The more tangible depletion of CaO relative to Na_2O and K_2O indicates that upon decomposition of feldspars, some proportions of K and Na were fixed by sericite and paragonite.

7 The conversion of the early-stage alteration (potassic and propylitic) assemblages into transitional (phyllic) and ultimately into the late argillic ones was concomitant with the decrease in activities of K^+, Mg^{2+}, and other cations relative to H^+ in the hydrothermal fluids.

Acknowledgements

This contribution is a part of the first author's PhD thesis. The laboratory works were carried out at the Institute of Mineralogy and Economic Geology, RWTH Aachen University, Germany. Funding for this project was provided by the Ministry of science, research and technology, Iran. Grateful appreciation is futher extended to Dr. Andre Hellmann for his assistance in whole-rock geochemistry analyses. Thanks go to B. Ahin for giving us the permission to have access to core log samples. Special thanks are also expressed to Prof. Antonio Gianfagna for his editorial assistance and to anonymous reviewers for making critical comments on this paper.

References

Ahmad S.N. and Rose A.W. (1980) - Fluid inclusions in porphyry and skarn ore at Santa Rita, New Mexico. *Economic Geology*, 75, 229-250.

Alavi M. (1991) - Sedimentary and structural characteristics of the Paleo-Tethys remnants in northeastern Iran. *Geological Society of American Bulletin*, 103, 983-992.

Aiuppa A., Allard P., D'Alessandro W., Michel A., Parello F., Treuil M. and Valenza M. (2000) - Mobility and fluxes of major, minor and trace metals during basalt weathering and groundwater transport at Mt. Etna volcano (Sicily). *Geochimica et Cosmochimica Acta*, 64 (11), 1827-1841.

Baumgartner L.P. and Olsen S.N. (1995) - A least-square approach to mass transport calculations using the isocon method. *Economic Geology*, 59, 1261-1270.

Beane R.E. and Titley S.R. (1981) - Porphyry copper deposits, alteration and mineralization, part II. *Economic Geology*, 75, 235-269.

Berberian M. (1973) - Structural history of Lut Zone. Geological Survey of Iran, Tehran, Internal Report. 34 pp.

Berberian M. and King G CP. (1981) - Toward a pale geography and tectonic evolution of Iran. *Geology survey of Iran, Report No*. 52, 502-557.

Berberian M. (1981) - Active faulting and tectonics of Iran, in Gupta, H. K., and Delany, F. M., editors, Zagros-Hindu Kush-Himalaya Geodynamic Evolution. *American Geophysical Union Geodynamic Series*, 3, 33-69.

Boomeri M. Nakashima K. and Lentz D.R. (2009) - The Miduk Porphyry Cu Deposit, Kerman, Iran: a petrologic analysis of the potassic zone including halogen element systematics related to Cu mineralization processes. *Journal of Geochemical Exploration*, 103, 17-29.

Bühl A. and Zöfel P. (1999) - SPSS version 8. Einführung in die Moderne Datenanalyse unter Windows: Bonn, Addison-Wesley Longmann.

Calagari A.A. (2003) - Concentration variations of major and minor elements across various alteration zones in porphyry copper deopsit at Sungun, East-Azarbaidjan, Iran. *Journal of Sciences, Islamic Republic of Iran,* 14(1), 27-36.

Calagari A.A. (2004) - Geology and fracture-related

hypogene hydrothermal alteration and mineralization of porphyry copper deposit at Sungun. *Journal of Geological Society of India*, 64(5), 595-618.

Chatziliadou M., Sindern S., Hilgers C. and Kramm U. (2005) - Spurenelementverteilung in Gesteinen der RWTH-1 Bohrung, Aachen. - Ber. Dt. Mineral. Ges.; Beih. *European Journal of Mineralogy*, 17(1), 22.

Cline J.S. and Bodnar R.J. (1991) - Can economic porphyry copper mineralization be generated by a typical calc-alkaline melt? *Journal of Geophysical Research*, 96, 8113-8126.

Davoudzadeh M. and Schmidt K. (1984) - A review of the Mesozoic paleogeography and paleotectonic evolution of Iran. *Neues Jahrbuch für Geologie und Palaontologie-Abhandlungen*, 168, 182-207.

Dilles J.H. and Einaudi M.T. (1992) - Wall-rock alteration and hydrothermal flow paths about the Ann-Mason porphyry copper deposit, Nevada. *Economic Geology*, 87, 1963-2001.

Grant J.A. (2005) - Isocon analysis: A brief review of the method and applications. *Physics and Chemistry of the Earth*, 30, 997-1004.

Grant J.A. (1986) - The isocon diagram: A simple solution to Gresens' equation for metasomatic alteration. *Economic Geology*, 81, 1976-1982.

Gresens R.L. (1967) - Composition-volume relationships of metasomatism. *Chemical Geology*, 2, 47-65.

Hawthorne F. (1981) - Crystal chemistry of the amphiboles; Mineralogy Society of America. *Reviews in Mineralogy*, 9, 1-102.

Hezarkhani A. (2006a) - Fluid Inclusion Investigations of the Raigan Porphyry Copper System, Kerman-Bam, Iran. *International Geology Review*, 48, 255-270.

Hezarkhani A. (2006b) - Mass Changes during Hydrothermal Alteration/Mineralization at the Sar-Cheshmeh Porphyry Copper Deposit, Southeastern Iran. *International Geology Review*, 48, 841-860.

Idrus A., Kolb J. and Meyer F.M. (2009) - Mineralogy, Lithogeochemistry and Elemental Mass Balance of the Hydrothermal Alteration Associated with the Gold-rich Batu Hijau Porphyry Copper Deposit, Sumbawa Island, Indonesia. *Resource Geology*, 59(3), 215-230.

Imai A. (2000) - Genesis of the Mamut porphyry Cu deposit, Sabah, East Malaysia. *Resource Geology*, 50, 1-23.

Imai A. (2001) - Generation and evolution of ore fluids for porphyry Cu-Au mineralisation at the Santo Tomas II (Philex) deposit, Philippines. *Resource Geology*, 51, 71-96.

Karimpour M.H. and Zaw K. (2000) - Geochemistry and physicochemical condition of Qaleh-Zari Cu-Ag-Au ore bearing solution based on chlorite composition. *Iranian Journal of Crystallography and Mineralogy*, 8, 3-22.

Karimpour M.H., Zaw K. and Huston D.L. (2005) - S-C-O Isotopes, Fluid Inclusion Microthermometry, and the Genesis of Ore Bearing Fluids at Qaleh-Zari Fe-Oxide Cu-Au-Ag Mine, Iran. *Journal of Sciences Islamic Republic of Iran*, 16 (2), 153-169.

Karimpour M.H., Stern C.R., Farmer L., Saadat S. and Malekezadeh A. (2011) - Review of age, Rb-Sr geochemistry and petrogenesis of Jurassic to Quaternary igneous rocks in Lut Block, Eastern Iran. *Journal Geopersia*, 1, 19-36.

Kirschbaum A., Martinez E., Pettinari G. and Herrero S. (2005) - Weathering profiles in granites, Sierra Notre (Cordoba, Argentina). *Journal of South American Earth Sciences*, 19, 479-493.

Kluyver H.M., Griffts R.J., Tirrul R., Chance P.N. and Meixner H.M. (1978) - Geological Quadrangle Map Sheet Lakar Kuh Quadrangle 1:250,000. Geology Survey of Iran 35 pp.

Leitch C.H.B. and Lentz D.R. (1994) - The Gresens approach to mass balance constrains of the alteration systems: methods, pitfalls, examples: in Lentz, D.R., eds., Alteration and alteration processes associated with ore-forming systems. *Geological Association of Canada, Short Course Notes*, 11, 161-192.

Lensch G. and Schmidt K. (1984) - Plate tectonic, orogeny, and mineralization in the Iranian fold belts results and conclusions. *Neues Jahrbuch für Geologie und Palaontologie. Abhandlungen* 168(2/3), 558- 568.

Lowell J.D. and Guilbert J.M. (1970) - Lateral and vertical alteration-mineralisation zoning in porphyry ore deposits. *Economic Geology*, 65, 373-408.

MacLean W.H. and Kranidiotis P. (1987) - Immobile elements as monitors of mass transport in hydrothermal alteration: Phelps Dodge massive sulfide deposit, Matagami. *Economic Geology,* 82, 951-962.

MacLean W.H. (1990) - Mass change calculations in altered rock series. *Mineralium Deposita*, 25, 44-49.

Mahmoudi S., Masoudi F., Corfu F. and Mehrabi B. (2010) - Magmatic and metamorphic history of the Deh–Salm metamorphic Complex, Eastern Lut block, (Eastern Iran), from U-Pb geochronology. *International Journal of Earth Sciences*. 99, 11153-11165.

Malekzadeh A. (2010) - Rb-Sr and Sm-Nd isotopic compositions and Petrogenesis of ore-related intrusive rocks of gold-rich porphyry copper Maherabad prospect area (North of Hanich), east of Iran. *Iran Journal of crystallography and mineralogy*, 18, 15-32.

Mazhari S.A. and Safari M. (2013) - High-K calc-alkaline plutonism in Zouzan, NE of Lut block, Eastern Iran: An evidence for arc related magmatism in Cenozoic. *Journal of the Geological Society of India*. 81, 698-708.

Nesbitt H.W. and Markovics G. (1997) - Weathering of granodioritic crust, long-term storage of elements in weathering profiles, and petrogenesis of siliciclastic sediments. *Geochimica et Cosmochimica Acta*, 61, 1653-1670.

Nabavi M. (1976) - An Introduction to the Geology of Iran. Geological Survey of Iran Publication, 109 pp (in Persian).

Niazi M. and Asoudeh I. (1978) - The depth of seismicity in the kermanshah region of the Zagros Mountains (Iran). *Earth and Planetary Science Letters*, 40, 270-274.

Pourhosseini F. (1981) - Petrogenesis of Iranian plutons: A study of the Natanz and Bazman intrusive complexes: Cambridge, University of Cambridge, UK, Unpub. Ph.D thesis, 315 pp.

Ramezani J. and Tucker R.D. (2003) - The Saghand region, centeral Iran: U-Pb geochronology, petrogenesis and implications for Gondwana tectonics. *American Journal of Science*, 303, 622-665.

Ranjbar H., Honarmand M. and Moezifar Z. (2004) - Application of the crosta technique for porphyry copper alteration mapping, using ETM+ data in the southern part of the Iranian volcanic sedimentary belt. *Journal of Asian Earth Sciences*, 24, 237-243.

Richards J.P., Spell T., Rameh E., Razique A. and Fletcher T. (2012) - High Sr/Y magmas reflect arc maturity, high magmatic water content, and porphyry Cu ± Mo ± Au potential: examples from the Tethyan arcs of Central and Eastern Iran and Western Pakistan. *Economic Geology*. 107, 295-332.

Rieder M., Cavazzini G., D`Yakonov Y.S., Frank-Kamentskii V.A., Gottardi G., Guggenheim S., Koval P.V., Müller G., Neiva A.M.R., Radoslovich E.W., Robert J.L., Sassi F.P., Takeda H., Selby D. and Nesbitt B.E. (2000) - Chemical composition of biotite from the Casino porphyry Cu-Au-Mo mineralisation, Yukon, Canada: Evaluation of magmatic and hydrothermal fluid chemistry. *Chemical Geology*, 171, 77-93.

Selverstone J., Morteani G. and Staude J.M. (1991) - Fluid channeling during ductile shearing: transformation of granodiorite into aluminous schist in the Tauern Window, Eastern Alps. *Journal of Metamorphic Geology*, 9, 419-431.

Shafiei B. and Shahabpour J. (2008) - Gold Distribution in Porphyry Copper Deposits of Kerman Region, Southeastern Iran. *Journal of Sciences, Islamic Republic of Iran*, 19, 247-260.

Shahabpour J. (2000) - Behavior of Cu and Mo in the Sar Cheshmeh porphyry Cu deposit, Kerman, Iran. *Canadian Institute of Mining and Metallurgy Bulletin*, 93, 44-51.

Siahcheshm K., Calagari A.A., Abedini A. and Lentz D.R. (2012) - Halogen signatures of biotites from the Maher-Abad porphyry copper deposit, Iran: characterization of volatiles in syn-to post-magmatic hydrothermal fluids. *International Geology Review*, 54(12), 1353-1368.

Siahcheshm K., Calagari A.A., Abedini A. (2014) - Hydrothermal evolution in the Maher-Abad porphyry Cu–Au deposit, SW Birjand, Eastern Iran: evidence from fluid inclusions. *Ore Geology Reviews*, 58, 1-13.

Sillitoe R.H. (1973) - Geology of the Los Pelambres porphyry copper deposit, Chile. *Economic Geology*, 68, 1-10.

Taghipour N., Aftabi A. and Mathur R. (2008) - Geology and Re-Os Geochronology of Mineralization of the Miduk Porphyry Copper Deposit, Iran. *Resource Geology*, 58(2), 1-18.

Tarkian M., Lotfi M. and Baumann A. (1983) - Tectonic, magmatism and the formation of mineral deposits in the central Lut, east Iran: Ministry of mines and metals. GSI, geodynamic project (geotraverse) in Iran, 51, 357-383.

Titley S.R. and Marozas D.C. (1995) - Processes and Products of supergene copper enrichment: in Porphyry copper deposits of the American Cordillera, *Arizona Geological Society Digest,* 20, Pierce, F.W. and Bolm, J.G., editors, 156-168.

Tirrul R., Bell L.R., Griffis R.J. and Camp V.E. (1983) - The Sistan suture zone of eastern Iran. *Geological Survey of America Bulletin*, 84, 134-150.

Ulrich T. and Heinrich C.A. (2002) - Geology and alteration geochemistry of the porphyry Cu-Au deposit at Bajo de la Alumbrera, Argentina. *Economic Geology*, 97, 1865-1888.

Whitney D.L. and Evans B.W. (2010) - Abbreviations for names of rock-forming minerals. *American Mineralogist*, 95, 85-187.

Submitted, December 2013 - Accepted, March 2014